

Article

Formaldehyde Continuous Monitoring at a Rural Station North of Rome: Appraisal of Local Sources Contribution and Meteorological Drivers

Francesca Vichi ^{*} , Cristiana Bassani , Antonietta Ianniello, Giulio Esposito, Mauro Montagnoli and Andrea Imperiali

Institute of Atmospheric Pollution Research, National Research Council of Italy, Strada Provinciale 35d, 9, Montelibretti, 00010 Rome, Italy; cristiana.bassani@iia.cnr.it (C.B.); antonietta.ianniello@iia.cnr.it (A.I.); giulio.esposito@iia.cnr.it (G.E.); mauro.montagnoli@iia.cnr.it (M.M.); andrea.imperiali@iia.cnr.it (A.I.)

* Correspondence: francesca.vichi@iia.cnr.it

Abstract: The formaldehyde (HCHO) dataset collected from January to December 2022 at the CNR Liberti Observatory (42.10° N; 12.64° E), a rural site located 30 km NE of Rome, is reported. The daily, weekly, and seasonal trends are examined. The highest average seasonal HCHO concentration (1.9 ppb) was measured during summer, whereas similar values (1.5 ppb) were found for winter and spring periods. The meteorological parameters monitored at the site allowed the interpretations of the maxima observed during the period investigated. The daily trends examined for the different seasonal periods, along with other pollutants available (NO₂, NO, and O₃), showed how the sources gradually shifted from primary to secondary. The occurrence of wildfires and other events in the area were also considered in explaining peak events (>4.2 ppb). The site examined was sometimes impacted by the nearby urban anthropic pressure of Rome, but in many cases, particularly during the summer months, the influence of the natural background surrounding the site was evident.

Keywords: formaldehyde; rural site; photochemical smog



Citation: Vichi, F.; Bassani, C.; Ianniello, A.; Esposito, G.; Montagnoli, M.; Imperiali, A.

Formaldehyde Continuous Monitoring at a Rural Station North of Rome: Appraisal of Local Sources Contribution and Meteorological Drivers. *Atmosphere* **2023**, *14*, 1833. <https://doi.org/10.3390/atmos14121833>

Academic Editors: Xiao Sui, Daiqi Ye and Yoshiteru Iinuma

Received: 18 October 2023

Revised: 1 December 2023

Accepted: 7 December 2023

Published: 18 December 2023



Copyright: © 2023 by the authors. Licensee MDPI, Basel, Switzerland. This article is an open access article distributed under the terms and conditions of the Creative Commons Attribution (CC BY) license (<https://creativecommons.org/licenses/by/4.0/>).

1. Introduction

Formaldehyde (HCHO) is one of the most abundant carbonyl compounds in the air, which has an active role in atmospheric chemistry, leading to the formation of important oxidants, such as ozone (O₃), and smog components as secondary organic aerosol (SOA) [1]. Formaldehyde was classified in 2004 as a Group 1 carcinogen for humans by the International Agency for Research on Cancer [2] EU Regulation (EU 2015/491) [3] revised, as well, the classification of formaldehyde from suspected carcinogen to carcinogen for humans in category 1B, with the associated expression “it can cause cancer”, on the basis of the body of evidence collected [4]. Acute effects of this species include eye, nose, and throat irritation, further getting to worse symptoms (cough and bronchitis) if exposure to higher levels of formaldehyde occurs (<https://www.epa.gov/sites/default/files/2016-09/documents/formaldehyde.pdf> (accessed on 6 December 2023)) [5].

Most of the efforts in the study of this species were devoted over time to indoor environments because the exposure levels, due to the emission of materials employed in indoor furnishing, could possibly more easily reach values of concern for health preservation [6,7], but the importance of formaldehyde, in general, on atmospheric processes was also increasingly highlighted by a remarkable number of studies [8–10] and recently the interplay between indoor/outdoor sources was also evaluated [11,12]. Finding the contribution of both primary and secondary sources, respectively, on the release and formation of HCHO in different environments, indeed, has been the subject of observations during the last several years in urban [13–15] and rural or remote sites [16–18].

Among the sources, industrial emissions (chemical and petrochemical facilities, paints and solvents production, plastic manufacturing), vehicular traffic (diesel, biofuels, or natural gas-fueled vehicles) [19], and wastewater treatment processes are the most impacting anthropogenic emissions, but a not negligible contribution from natural sources should also be accounted for. Biogenic Volatile Organic Compounds (BVOCs) are precursors of Oxygenated Volatile Compounds (OVOCs) [20] and, along with biomass burning, can be the most important sources, especially in rural environments.

Up to 50% of the formaldehyde mixing ratio in urban areas is of primary origin during winter [21], but in other areas, the largest fraction of atmospheric HCHO is of photochemical origin, depending on the season, climatic conditions, and vegetation cover. The mechanisms of HCHO formation have been studied and are well known [9,22]: oxidation of alkenes by ozone, the reaction of alkanes, alkenes, and aromatics with OH radicals and nitrogen oxides during the day, and with nitrate radical (NO₃) during the night. The reactive species are in some cases of anthropogenic origin or can be emitted by vegetation, e.g., isoprene and terpenes; the latter are involved in a cycloaddition reaction with O₃ to form energy-rich intermediates that undergo a fast fragmentation, giving HCHO. Thermal decomposition of cellulose-containing materials in biomass combustion and combustion of biofuels are also other important pathways of formation [23].

The relative contribution of the different sources depends on many factors, location and season being the most important, and the task of accounting for a primary or secondary origin is quite complex. As remarked by Parrish [13], a suitable correlation of HCHO with species directly emitted by anthropogenic sources (such as SO₂, CO) or photochemically produced (such as O₃ and PAN) per se is not robust enough to prove that HCHO has the same origin. The direct emissions of other VOCs by the same sources can, indeed, be the cause of such suitable correlation, and a successive secondary formation can also be hypothesized as responsible for HCHO production.

Confounding effects affecting HCHO mixing ratios during different periods of the day due to the diverse loss rates (caused mainly by photolysis during the day as well as by dry and wet deposition in different seasons) [20], to atmospheric dilution or, in certain cases to transport, should be considered when attempting to attribute HCHO to different sources.

Measurements of HCHO have been conducted over the years, at first employing discontinuous sampling on DNPH-coated cartridges and, more recently, by automatic instruments providing real-time data. In the early 1990s, at six remote stations of the European Monitoring and Evaluation Programme (EMEP) network located across Europe (Birkenes, Mace Head, Waldhof, Kosetice, Donon, and Ispra), measurements were carried out for an entire year by DNPH cartridge collection and successive analysis and compared with modeled data as reported by Solberg [24]. Largiuni [25] performed continuous measurements in Florence by means of a homemade spectrofluorimetric instrument based on the Hantzsch reaction. Other more recent studies were conducted by Balzani [26] at the Jungfraujoch (3580 m a.s.l.) and by Leuchner [17] at the Environmental Research Station Schneefernerhaus (UFS) (2650 m a.s.l.), in both the cases the measurements were performed on a seasonal basis by a commercial Hantzsch monitor. These assessments were aimed at the evaluation of HCHO in the free troposphere. The rural site of Mazhuang in the Shandong province was monitored by Wang [27] using a scrubbing DNPH-containing solution, analyzed continuously by an HPLC instrument. Assessments in rural environments were conducted by de Blas [20] in the Valderejo Natural Park in northern Spain in the summer of 2016 by the same Hantzsch monitor. Other peculiar background sites were those monitored by Rocco [18], who carried out a study at Reunion Island on three different sites (an observatory at 2200 m, at a site in the tropical forest, and in an urban area) and Preunkert [16], who reports ambient air levels as well as HCHO fluxes on the snow at the Concordia site, located near Dome C on the East Antarctic Plateau.

In this study, the analysis of the HCHO dataset was obtained using a commercial Aero-Laser formaldehyde analyzer at the Liberti Observatory (42.10° N; 12.64° E), a rural site located in the RM1 Research Area of the Italian National Research Council (CNR), at

about 30 km NE of Rome is reported. The correlation among the different pollutants, i.e., nitrogen dioxide (NO_2), nitrogen oxide (NO), and ozone (O_3), is considered, as well as the meteorological parameters collected locally and the transport mechanisms employing backward trajectories. The availability of highly time-resolved data provided by an automatic analyzer allows an in-depth analysis of the modulation of the mixing ratios during the day and as the season changes. The assessment of the HCHO levels at rural sites is of utmost importance to understand the pathways of the formation of ozone, which tends to reach particularly high levels in these areas, providing useful information on the contribution of transport and local emissions, which can help in air quality management when planning mitigation measures. This is of paramount interest also in light of the recent efforts in reviewing the EC Directive 2008/50, which foresees the extension of ozone precursors monitoring to many more species than previously required (<https://eur-lex.europa.eu/legal-content/EN/TXT/DOC/?uri=CELEX:52022PC0542> (accessed on 6 December 2023)) [28].

2. Materials and Methods

2.1. Sampling Site

In this study, simultaneous HCHO, NO_x , and O_3 measurements carried out from 15 January to 31 December 2022 at the “Arnaldo Liberti” Observatory ($42^\circ 06' 38''$ N, $12^\circ 38' 05''$ E; 48 m a.s.l.), an experimental facility of the National Research Council (CNR) (Figure 1), inside of Research Area RM1 in Montelibretti (Rome, Italy) are reported.

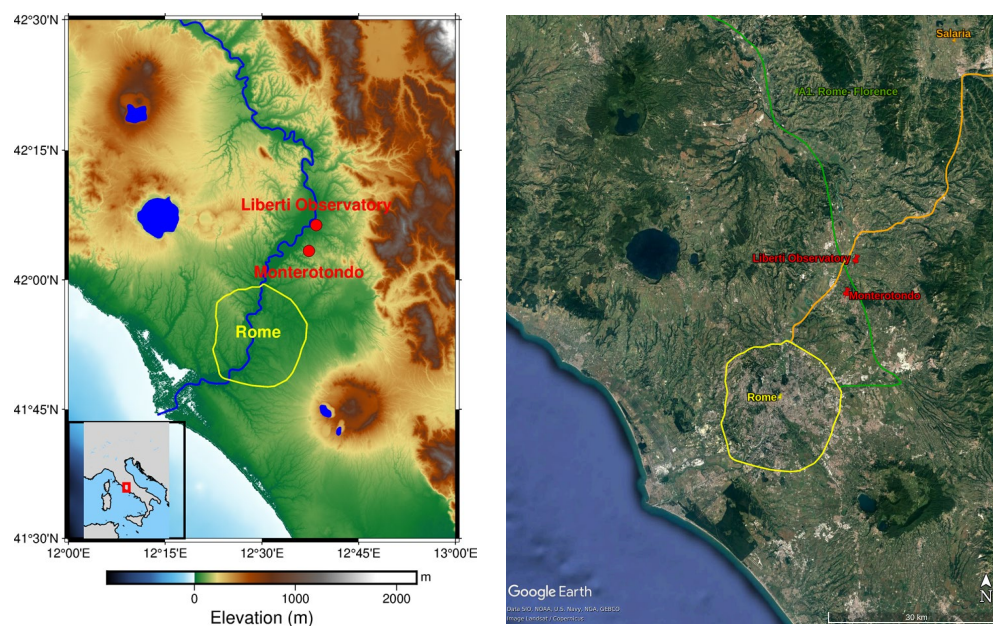


Figure 1. Location of the Liberti Observatory: on the left is the topographic map of the area; on the right is the satellite view.

The station is located in a rural area of the Tiber Valley, about 30 km northeast of Rome and approximately 45 km northeast of the Tyrrhenian coast. Although regarded as a regional background site, it is occasionally influenced by anthropogenic emissions of the metropolitan area of Rome, with about 2,748,599 inhabitants in 2022 (<https://demo.istat.it/app/?a=2022&i=D7B> (accessed on 6 December 2023)) [29], transported at the site by sea–land breeze circulation system [30,31] (Ciccioli et al., 1999; Brines et al., 2015). This site is affected by local emissions due to the presence of agricultural activities and biomass domestic heating appliances surrounding the station, by Monterotondo town with about 41,000 inhabitants, at about 5 km west–southwest, and by heavy traffic roads as a major highway (A1 Rome–Florence), at about 2 km west, and a primary route (Via Salaria, SS4) not far from Pianabella railway station, 400 m away from the station [32,33]. The site is

also an EMEP station, where the transport and transformation of atmospheric pollution generated in the urban area of Rome can be evaluated [34].

The area in which the observatory is located is halfway from Monterotondo's outskirts and nearby rural areas mainly devoted to agriculture and farming. In the neighborhoods of the measurement site, just outside the residential part of Monterotondo, an industrial area holding logistic facilities, typographic activities, building and finishing products warehouses, and small workshops is present. Agricultural product processing activities, on the other hand, are also present, sparse in the whole Sabina area (the historical region on the left side of the Tiber river, northeast of Rome) where oil production through many different oil mills is one of the major activities, and wine production is another important sector. On the whole, the area is not affected by single industrial emissions but rather by small sources mainly related to the residential and services industries.

2.2. On-Line Formaldehyde Analyzer

The continuous formaldehyde measurements were performed at Liberti Observatory using a commercially automatic analyzer (AL4021, Aero-Laser GmbH, Garmisch-Partenkirchen, Germany). The instrument is based on the Hantzsch reaction with fluorescence detection [35,36]. Firstly, the gaseous formaldehyde is quantitatively stripped into a sulphuric acid solution (H_2SO_4 0.054 M) through a stripping coil at a constant temperature of 10 °C and at defined flow rates (1 L/min for gas and 0.45 mL/min for stripping solution). Under these conditions, the stripping efficiency is about 100%, as indicated by the Aero-Laser producer (<https://www.aero-laser.de/fileadmin/downloads/AL4021-manual-Rev.2.2.pdf> (accessed on 6 December 2023)) [37]. Consecutively, the Hantzsch reaction takes place in a heated reactor coil at 68 °C in which the resultant aqueous formaldehyde reacts with acetyl acetone (2–4 pentadione) and ammonia (NH_3) producing 3,5-diacetyl-1,4-dihydrolutidine (DDL). This product absorbs light at 410 nm and shows a strong fluorescence at 510 nm. The use of the Hantzsch reaction in combination with fluorescence detection increases the sensitivity and selectivity to HCHO determination and decreases cross-sensitivity to other aldehydes and ketones and other interfering species [38,39]. Approximately every ten days, when changing the stripping and Hantzsch reagent solutions, the instrument is calibrated with liquid standards freshly prepared by diluting a 10^{-2} M HCHO stock standard with the stripping solution. In addition, daily automated zeroing measurements are performed for about 20 min by passing the sampled air through an internal zero catalyst trap [40]. The internal software of the instrument uses the last zero measurement to evaluate the current measurement. The time response of the instrument is about 90 s (10% to 90%), with an additional time delay of 300 s due to the time required to transport the liquid from the coil to the fluorimeter. The detection limit of the instrument, defined as 2 times the standard deviation, is 100 ppt, and the operativity concentration range is linear up to 3 ppm. These features made this instrument attractive for the sampling site, which is a rural station, where the expected concentration values can reach very low levels.

2.3. Additional Measurements

Continuous and simultaneous ozone (O_3) measurements were performed every 1 min by a Teledyne API (Model T400, Teledyne API, San Diego, CA, USA) based on the well-established European standard technique of absorption of ultraviolet light at 254 nm (EN 14625:2012) [41]. The quantity of light absorbed over a certain distance at a given temperature and pressure is proportional to O_3 concentration according to the Beer–Lambert law. The detection limit of this analyzer is 0.4 ppb, and the measurement precision is 0.5%.

NO_x was monitored in parallel every 1 min using a chemiluminescence analyzer (Model 200E, Teledyne Instruments, San Diego, CA, USA) with a detection limit of 0.4 ppb and a measurement precision of 0.5%. The chemiluminescence analyzers use the intensity of the light produced by the reaction of NO with O_3 molecules, peaking at 630 nm. By converting NO_2 to NO (molybdenum converter), the total NO_x value can be calcu-

lated, allowing the determination of NO, NO₂, and total NO_x. The chemiluminescence method is a European standard technique for measuring atmospheric nitrogen oxides (EN 14211:2012) [42].

All gas calibrations and gas test quality control concentrations for NO_x and O₃ measurements were obtained every week by dynamic dilution of gas from cylinders whose contents are traceable to NIST standards.

During the period investigated, the data were collected by the automatic analyzers on a minute basis, and then 5 min average values were calculated. To account for data losses or incompleteness, the time coverage of the timeframe considered (5 min) was taken into account among the different procedures adopted in the management of the monitoring station dataset. Meteorological parameters were monitored by a conventional weather station (Lsi Lastem s.r.l., Milan, Italy). The station, equipped with sensors for temperature, pressure, relative humidity, global solar radiation, and UVA and UVB light, is located at about 5.5 m a.g.l upon the roof of a container. Wind speed and direction were monitored by a sonic anemometer (DMB305, Lsi Lastem s.r.l., Milan, Italy) installed on a ten-meter pole located near the meteorological station. A datalogger (e-log Lsi Lastem s.r.l., Milan, Italy) stored the data acquired in real time into a 1 min average. These data were then averaged on a 5 min basis.

2.4. HYSPLIT Backward Trajectories

The backward trajectories were calculated with a runtime of 24 h at 500 m a.s.l. using the HYSPLIT transport model (https://www.ready.noaa.gov/HYSPLIT_traj.php (accessed on 6 December 2023)) [43] and the Global Forecast System (GFS) with a resolution of 0.25 degrees to determine the origin of air masses transported at the sampling site during this study.

3. Results and Discussion

3.1. Meteorological Conditions during the Study Period

The main meteorological parameters collected at the site are reported in Table 1.

The period under examination comprises almost all of the year 2022 (from 15 January to 31 of December). The four seasons were all monitored, with two periods missing some data. Some days are missing in winter since the measurements began on 15 of January, and in summer from 13 to 21 of August due to technical problems.

From hereafter, the seasonal periods considered will include three months each, starting from January and ending in December 2022. Over the entire period, the temperatures varied from -2.7 °C in January to 41.2 °C at the end of June. An opposite trend was observed, as expected, for the relative humidity (RH), which decreased as the season changed, from 90.5% in December to 55.4% in June, thus remaining, on average, at quite appreciable levels. The minimum levels of RH were recorded in June, the hottest month of the period when a value of 14.5% was observed. Generally, on the whole, the year 2022, with a total of 637.4 mm of precipitation, was in line with the mean of the precipitation records in the area of the last 20 years [44]. The month of May was rainier than the previous months with most of the precipitation recorded during a single event on 27 of May (42.2 mm of precipitation recorded). The autumn was, as expected, characterized by more abundant total precipitations (318.6 mm) and an average temperature of 15.1 °C. The global radiation showed a slow decline from 235.6 W/m² in September to 97.7 W/m² in December, and the winds recorded were also weaker than in summer, particularly during October and December.

In Figure 2, the wind roses plots are reported on a seasonal basis. The wind records showed that the prevailing direction was from the north during all the seasons, accompanied by south–southwestern winds during spring and summer, which were then the dominant directions during the early summer months of June and July (see Figure S1f,g). These latter are sea breezes coming from the direction of the Tyrrhenian Sea, which is about 50 km far from the measurement site. The advection of air masses due to the periodic sea–land circulation is of great importance for the transport of polluted air masses from

Rome [45,46]. From August (see Figure S1h), the prevalent wind direction slowly returned to be northerly, and during the following autumnal months, it was accompanied by an easterly component.

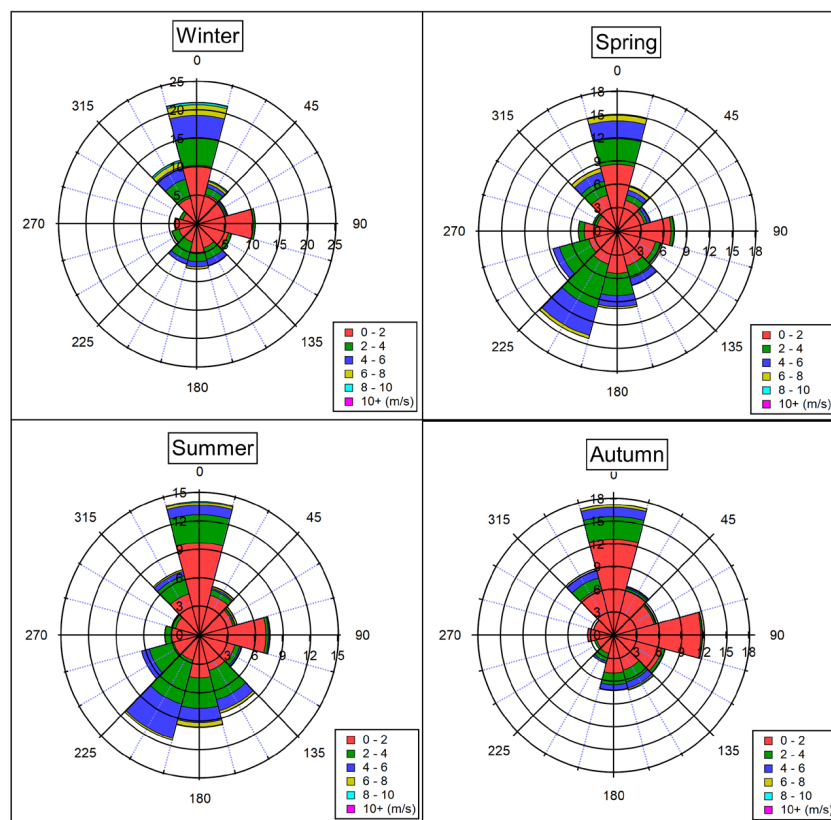


Figure 2. Wind roses relative to the seasonal periods during the year investigated.

The stronger winds, on an average monthly basis, were recorded during the month of February, when a wind speed (WS) of 2.4 m/s was observed. More detailed plots regarding specific events are reported in Section 3.2.

3.2. Formaldehyde Trends and Correlations among Collected Data

The dataset collected was comprehensive of HCHO and other pollutants more widely monitored as NO₂, NO, and O₃.

The basic statistical parameters of the whole dataset are reported in Table 2.

The data coverage over the year ranged from 96% for certain meteorological parameters (precipitation and UV radiation) to 90–92% for pollutants data; as mentioned previously, HCHO data are lacking in two periods in winter and summer, therefore, data coverage in this case was 84.1%.

The average value of the concentration of HCHO over the whole year was 1.5 ppb, with a maximum value of 15 ppb recorded in July. Taking into account the different sampling methodologies applied, the concentration ranges found in this study are comparable with previous assessments. Indeed, former HCHO measurements carried out at the Liberti Observatory for an 8 h sampling period by means of annular denuders on 23 June 1999 found values of 4.6 ppb (5.8 µg/m³) [47] and later in the period May–June 2002 concentrations varying between 2 and 12 ppb were reported [48], for collection periods from 3 to 5.5 h on DNPH cartridges. Successive measurements were performed at the same site in the periods July–September 2005 and February 2006 by means of cartridges collecting 8 h samples (from 8.00 to 16.00) [32]. During these more extensive campaigns, in which HCHO was measured with many other carbonyls, the values found ranged from a maximum of 7 ppb in July to a minimum of 1.1 ppb in February.

Table 1. Monthly averages of the meteorological parameters during the period investigated.

Month	N	T (°C)	T _{MAX} (°C)	T _{min} (°C)	N	RH (%)	N	P (hPa)	N	Glob. Rad. (W/m ²)	Glob. Rad.-MAX (W/m ²)	N	UVA (W/m ²)	UVB (W/m ²)	N	WS (m/s)	WS _{MAX} (m/s)	WS _{min} (m/s)	N	Rain (mm)
January (15–31)	4886	7.7	18.0	−2.6	4886	78.2	4886	1025.4	647	380.6	696.36	4886	6.9	0.2	4884	2.0	9.9	<0.5	4886	5.8
February	8055	10.4	20.7	−1.3	8055	73.3	8055	1023.2	4335	238.1	1011.52	8055	8.8	0.2	7983	2.3	13.5	<0.5	8055	26.8
March	8109	10.8	23.8	−1.0	8101	62.9	8106	1024.8	8919	227.9	1050.28	8919	11.3	0.2	8907	2.1	10.4	<0.5	8919	29
April	8009	14.3	26.9	1.34	8009	67.2	8007	1016.5	8639	285.6	1372.78	8637	15.0	0.2	8335	2.4	9.7	<0.5	8639	26.2
May	8923	20.9	35.4	7.2	8915	65.6	8921	1019.4	8919	317.5	1385.08	8919	16.8	0.2	8802	1.8	11.1	<0.5	8919	48.4
June	8639	26.3	41.2	14.8	8639	55.4	8639	1018.0	8639	357.5	1264.78	8639	18.8	0.2	8202	2.0	12.5	<0.5	8639	30
July	6118	27.9	39.8	15.9	6118	55.9	6114	1018.3	8927	374.6	1321.6	8927	19.7	0.2	6375	1.9	16.1	<0.5	8927	46.8
August	8924	27.1	39	16.9	8897	61.4	8924	1015.7	8897	311.2	1242.88	8897	16.8	0.2	8485	2.0	16.0	<0.5	8866	26.8
September	8639	22.4	35.4	9.9	8639	70.8	8639	1016.5	8639	235.6	1149.52	8639	13.1	0.2	8197	2.0	10.4	<0.5	8639	130
October	8928	18.8	29.0	7.9	8928	79.1	8928	1025.4	8928	197.7	1019.74	8928	10.7	0.2	8427	1.0	6.8	<0.5	8928	17.8
November	8639	13.7	26.9	3.3	8639	81.5	8639	1018.0	8639	123.2	801.82	8639	7.3	0.2	8480	1.9	10.5	<0.5	8639	109
December	8926	11.7	20.4	1.5	8926	90.5	8926	1020.2	8926	97.7	666.95	8926	6.1	0.2	5908	1.0	8.6	<0.5	8926	140.8

The data are averaged on the 5 min based data. Max. = maximum; Min. = minimum; N is the number of data (referred to as the successive parameter in the table).

Table 2. Basic statistical treatment on the dataset.

Month	HCHO (ppb)					NO ₂ (ppb)					NO (ppb)					O ₃ (ppb)				
	N	Ave.	St. Dev.	Max.	Min.	N	Ave.	St. Dev.	Max.	Min.	N	Ave.	St. Dev.	Max.	Min.	N	Ave.	St. Dev.	Max.	Min.
January	4541	1.7	1.1	14.0	0.1	4884	9.0	5.7	44.1	0.4	4884	2.8	5.2	80.6	0.4	4618	16.2	11.8	45.5	0.5
February	7509	1.3	0.8	9.7	0.1	7989	6.8	5.2	35.2	0.4	7984	1.5	3.0	39.1	0.4	7984	23.5	12.7	48.2	0.9
March	8425	1.5	0.8	8.9	0.1	8928	5.2	4.0	35.1	0.4	8928	1.0	1.8	44.8	0.4	8928	31.7	14.1	66.4	1.6
April	8028	0.9	0.6	5.7	0.1	8335	3.2	2.8	24.3	0.4	8335	0.8	1.6	42.5	0.4	8332	32.0	13.5	67.8	1.2
May	8570	1.4	0.9	6.7	0.1	8621	3.4	2.8	22.1	0.4	8621	0.8	1.8	36.9	0.4	8759	32.8	17.4	93.0	1.9
June	7994	2.3	1.0	7.3	0.1	8371	3.2	2.4	20.5	0.4	8371	0.7	0.9	20.8	0.4	8331	37.4	17.5	95.6	2.1
July	8468	2.4	1.0	15.0	0.1	8840	3.6	2.6	19.2	0.4	8840	1.0	1.4	26.4	0.4	8748	39.5	19.5	96.1	1.6
August	5687	1.9	0.9	5.8	0.1	8479	3.7	2.2	18.5	0.4	8479	1.0	1.9	32.0	0.4	8489	38.5	18.9	83.7	1.5
September	8365	1.2	0.7	7.3	0.1	8497	4.3	3.3	28.9	0.4	8497	1.3	2.1	43.7	0.4	8441	29.6	14.8	76.1	1.3
October	8757	1.1	0.8	4.4	0.1	8202	6.4	4.0	37.4	0.4	8202	2.6	4.8	66.8	0.4	8355	19.5	14.0	56.2	0.4
November	8174	1.0	0.7	7.0	0.1	8310	6.7	4.5	38.9	0.4	8304	2.8	4.4	66.5	0.4	8347	17.0	11.3	48.4	0.8
December	3851	0.8	0.6	4.8	0.1	5922	6.1	3.5	29.0	0.4	5892	4.7	5.2	50.2	0.4	7649	11.7	10.1	64.3	0.4
Year	88,369	1.5	0.8	8.1	0.1	95,378	5.1	3.6	29.4	0.4	95,337	1.8	2.8	45.9	0.4	96,981	27.5	14.6	70.1	1.2

Abbreviation key: N = number of data; Ave. = average; St. dev. = standard deviation; Max. = maximum; Min. = minimum. The average value was calculated starting from 5 min averaged data.

Analyzing the trends of HCHO and of the other pollutants during the period under investigation, the correlation of the different species with HCHO was tested, and O₃ showed the highest correlation ($R^2 = 0.72$), followed by NO₂ ($R^2 = 0.46$) and NO ($R^2 = 0.10$). In addition, the correlation between HCHO and O₃ was steadily increasing from January ($R^2 = 0.34$) to August ($R^2 = 0.90$), and this observation could point to a secondary nature of an increasing portion of HCHO concentration, then gradually decreasing until December ($R^2 = 0.52$). This finding will be, as mentioned in the introduction, also considered in the light of meteorological data, backward trajectories, and local observations of particular events. Nevertheless, the predominant secondary nature of formaldehyde in certain seasonal periods is also supported by the highest average value and the highest maximum found in the month of July. Furthermore, the availability of a set of parameters, such as other atmospheric gas concentration and meteorological data monitored at the Liberti Observatory, allowed the extension of the assessment of the correlation on other parameters of the dataset, giving a wider perspective on data interpretation.

The correlation among different parameters was tested; the dataset taken into account included varying numbers of data (winter: 13,901 < N < 21,860; spring: 24,592 < N < 26,197; summer: 22,520 < N < 26,463; autumn: 20,782 < N < 26,493). By checking Pearson’s correlation among the data collected, the results reported in Figure 3 were obtained.

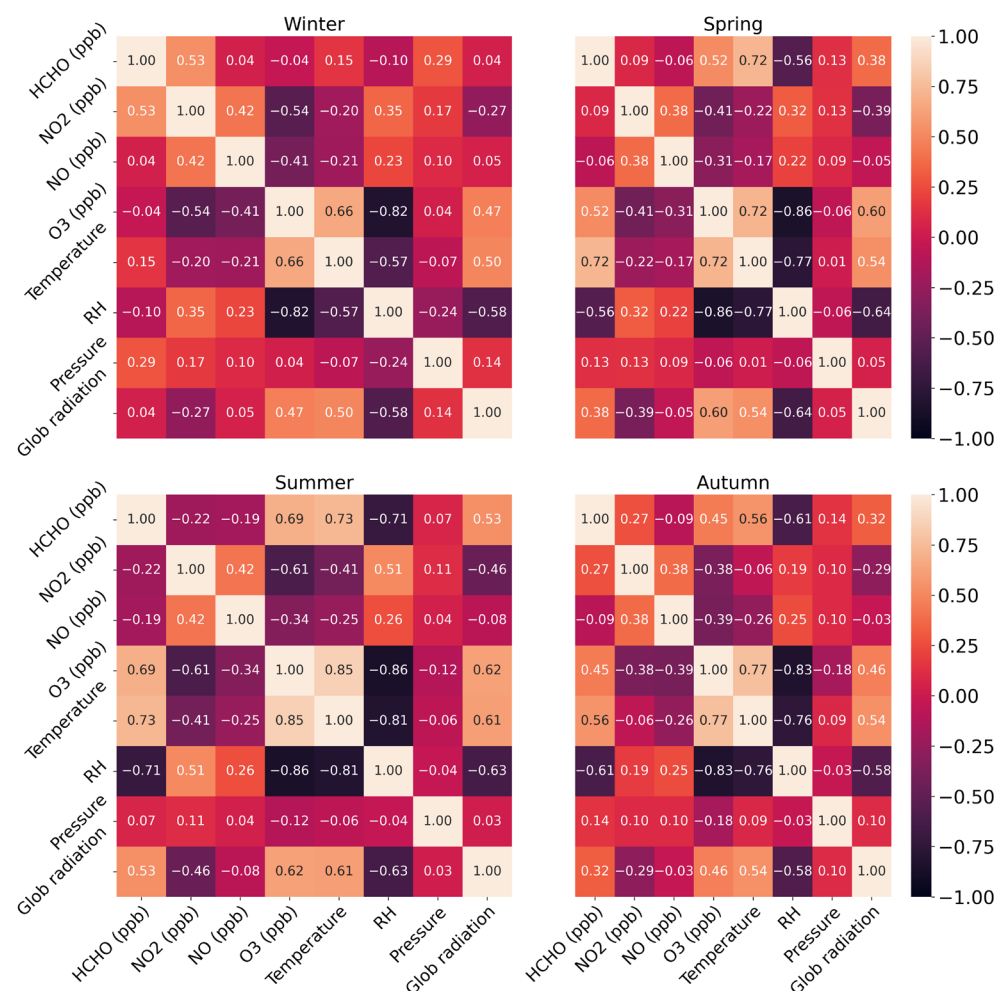


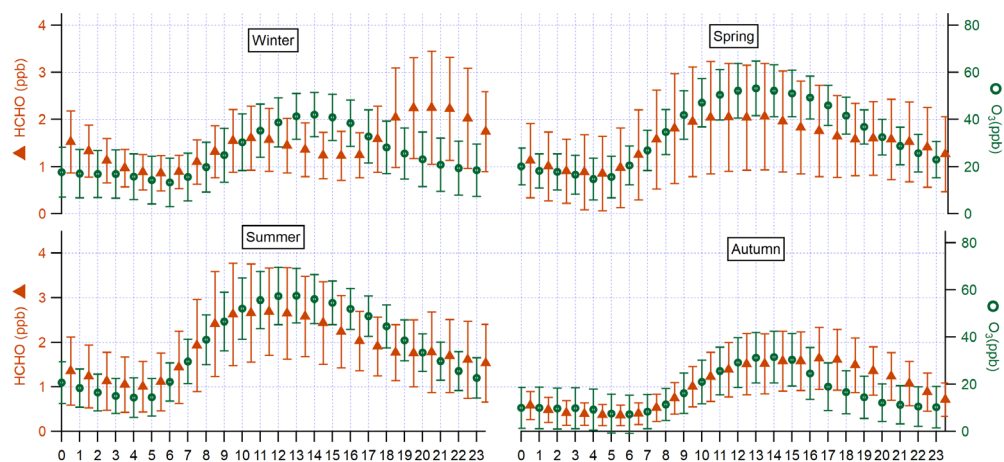
Figure 3. Seasonal correlation patterns (Pearson’s r) of pollutants and main meteorological data.

From the plots reported, it can be observed how both the correlation of HCHO vs. O₃ and HCHO vs. Global radiation increased until the summer period, later decreasing during the autumnal period. The opposite was observed for the correlation of HCHO vs. NO₂, which was at a minimum during the summer and a maximum in winter. As for O₃

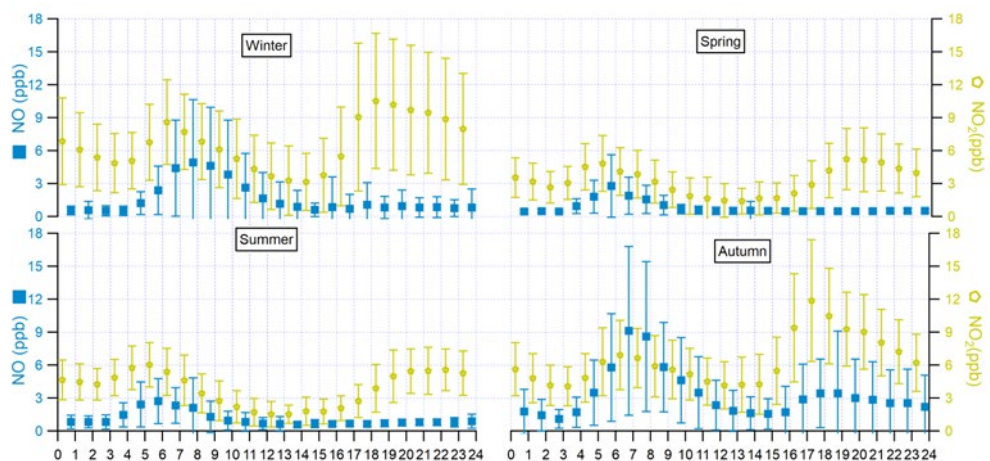
vs. Global radiation, O_3 vs. Temperature, and O_3 vs. RH, they keep the same correlation for the whole period. These findings strengthen the hypothesis of two distinct sources of HCHO, more related to primary sources during cold months and to photochemical patterns of formation during late spring and summer months.

3.2.1. Daily and Weekly Cycles of the Pollutants

From the analysis of the diel cycles, reported in Figure 4A, obtained by plotting the average hourly concentration, it is possible to observe how, during the period investigated, the highest hourly average value of HCHO was found during winter evening hours and during summer morning hours.



(A)



(B)

Figure 4. Seasonal diurnal variations of the pollutants (hourly averages are reported): (A) HCHO vs. O_3 , (B) NO_2 vs. NO.

The trends of HCHO and O_3 were quite different during winter since a bimodal distribution with a less pronounced morning peak at 10.00 UTC, followed by a rapid decrease to values around 1 ppb, and a second evening broad peak at 20.00–22.00 was observed for HCHO, whereas a unimodal distribution centered at lunchtime (13.00–14.00 UTC) was typical of O_3 .

In spring, the two distributions slowly became more similar, and during the month of May, a unimodal distribution was found for both, with a wide maximum starting from

10.00 UTC and declining from 18.00 UTC. HCHO distribution became once again unimodal in September, peaking at 12.00, and in October, peaking at 14.00, whereas during the autumn, a bimodal trend could be observed with a second evening peak at 17.00 (see Figure S2 for monthly daily cycles).

In Figure 4B, the daily trends of NO₂ and NO are reported, and the typical bimodal distribution with maxima in the early morning (6.00 UTC) and late afternoon (17.00–18.00 UTC) were observed during winter and early spring, the time of maxima occurrence varied over the year, gradually shifting to 5.00 UTC and to 19.00–20.00 UTC in spring and summer. The maxima concentration values gradually decreased during the late spring and summer periods for both pollutants. Then, during the autumn, the concentration, as expected, rose again, showing the typical bimodal trend peaking in the mornings at 6.00 and in the evenings at 17.00.

To better characterize the possible pollution sources, the weekly cycles can be of help since, as is well known, the vehicular traffic sources can significantly vary on weekdays (WD) and weekend periods (WE), affecting the overall air quality [49,50]. In Figure 5, it is apparent that in winter, there is a different behavior of HCHO and NO₂ since the latter decreases during weekends, whereas the former does not.

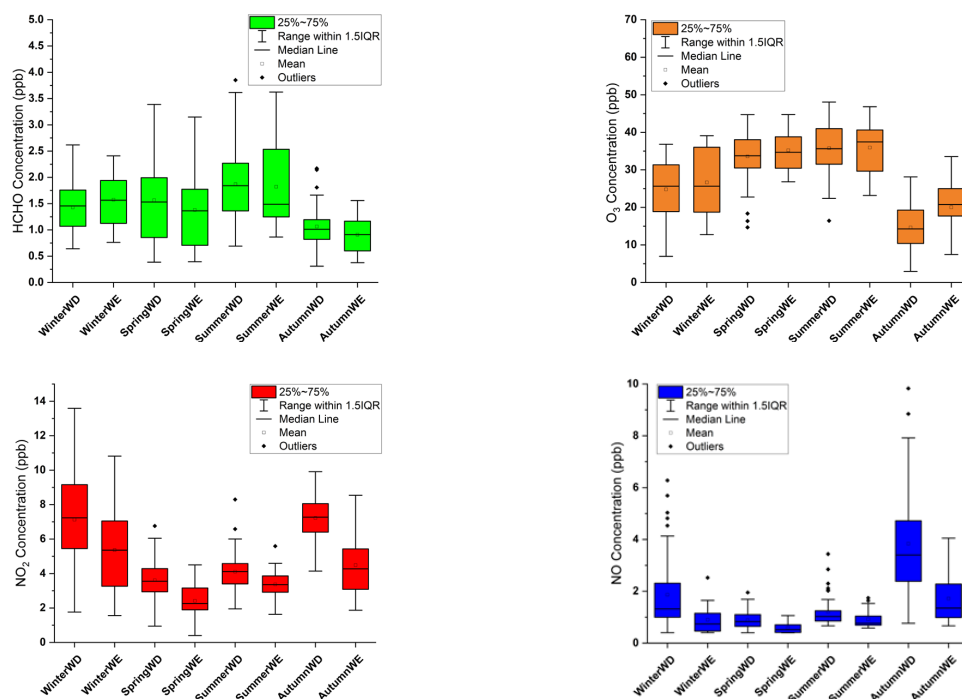


Figure 5. Box plot graphs of weekly cycles of the pollutants measured (WD: weekdays from Monday to Friday; WE: weekend days Saturday and Sunday).

HCHO's weekly cycle in spring and in summer shows small differences among the medians, particularly in summer, whereas NO₂ and NO both show a decrease during the weekends, sharper in spring than in summer. During autumn, the weekend effect becomes, again, evident for nitrogen oxides, whereas HCHO does not show appreciable differences between weekends and weekdays. A possible explanation of these findings is that the sources of HCHO differ during the two seasons, being most likely related to primary sources in winter and secondary sources in summer, as already hypothesized. It can be presumed that vehicular traffic is not the main primary source of HCHO during winter due to the different trends found for NO₂ and HCHO and that other emissions, for instance, the use of domestic heating, probably also by biomass burning appliances, can be an alternative source during weekends in wintertime. This could likely also explain the evening peak found in winter daily cycles (at about 21.00). Data dispersion has an opposite trend for the two pollutants, being greater in the winter period for NO₂ and in the

summer period for HCHO due to the variation in primary emission sources and secondary formation mechanisms, respectively.

Applying statistical tests, two-sample *t*-test, and the Kolmogorov–Smirnov test, depending on the assessment of normality of the dataset, to the 5 min based data grouped according to the day of the week in each season, it was found that at the 0.05 level of significance no statistically significant differences between the means of WD and WE were found for HCHO in the whole period dataset, whereas there were always statistically significant differences for NO₂ and NO dataset. The O₃ data were also tested, and only in autumn a statistically significant difference was found.

Other studies also tried to investigate the weekly trend of this compound. Hassan [51] found a statistically significant ($p \leq 0.001$) difference between HCHO mean concentrations on weekdays and weekends in a suburban area (15 May City), approximately 35 km south of the center of Cairo, where the weekly trend was such that higher values were observed on weekdays. Biswas [52] performed a detailed study in Pune using the MAX-DOAS technique but could not find noticeable differences between weekdays and weekends.

3.2.2. Peak Events Observed during the Study Period

The occurrence of peak events in the period under study requires further investigation to better understand the mechanisms of emission and formation of this pollutant at the study site.

From the statistical treatment on the HCHO dataset, comprising 5 min data of the whole year, the outliers were those values exceeding the maximum of 4.2 ppb found within the range 1.5 IQR (interquartile range). These exceedances were analyzed, taking into account both wind direction and speed monitored locally and backward trajectories relative to the whole area to obtain a wider picture of the synoptic conditions. The backward trajectory starting height of 500 m was chosen because it ensures that the trajectory starts in the atmospheric boundary layer (ABL). Moreover, this level is a very common choice as users enter data in the model.

The location of the sources with respect to the monitoring site was investigated by means of bivariate polar plots described earlier by Carslaw [53] and reported in Figures S3–S5.

In addition, events impacting the area, such as wildfires, particularly frequent during the summer of 2022, were considered.

The peaks observed over the different seasons of this year were, in many cases, attributable to a common origin; several events were caused by local sources lying within 10 km southwest of the site in the Monterotondo area. The discrimination between local and more distant emissions coming from the metropolitan area was made, taking into account the provenance and strength of the winds and the concomitant peaks recorded for other pollutants. After analyzing the data collected over the whole year, the following causes of peak events were found: 1. Transport from adjacent areas; 2. Transport from metropolitan area; 3. Photochemical processing of locally emitted VOCs.

In Figure 6, apart from HCHO, other pollutant trends and global radiation are plotted, and the main events related to photochemical formation or due to transport from nearby or Rome metropolitan urban areas are reported. The general pattern of transport is described by backward trajectories reported cumulatively in Figure 7.

Based on the event analysis, it is possible to conclude that in several cases, the peaks were due to local sources placed in the direction of Monterotondo. This provenance was observed during winter when the peaks occurred on 15th January, accompanied by NO₂ peaks, in the evening hours, between 20.00 and 20.30 (UTC time) (Figures S3a and S4a) and on 16th of February, at about 19.00 UTC when 9.7 ppb HCHO was observed, mirrored by a coincident NO₂ peak (Figures S3e and S4e).

Some of these events happened during winter evenings, both on weekends and weekdays, so they could be due to domestic heating during the cold evenings, and possibly a contribution, especially during weekends, could also come from a “leisure” vehicular traffic due to recreational and entertainment activities.

Other events can be likely ascribed to nearby or very local sources located in different directions with respect to the site. On 30th January at 20.00, a remarkable peak of 14 ppb was observed, coming from surrounding areas located east of the site (Figures S3b and S4b). In other winter episodes, as on the 10th and 23rd of February, the sources were placed, respectively, south and southeast of the site (Figures S3d,f and S4d,f), whereas on 4th of February, local HCHO sources were present slightly north of the site. On 4th of February, two peaks were observed, the first of 6.7 ppb at 10.00 and successively at 10.15 a peak of 8.08 ppb (Figures S3c and S4c).

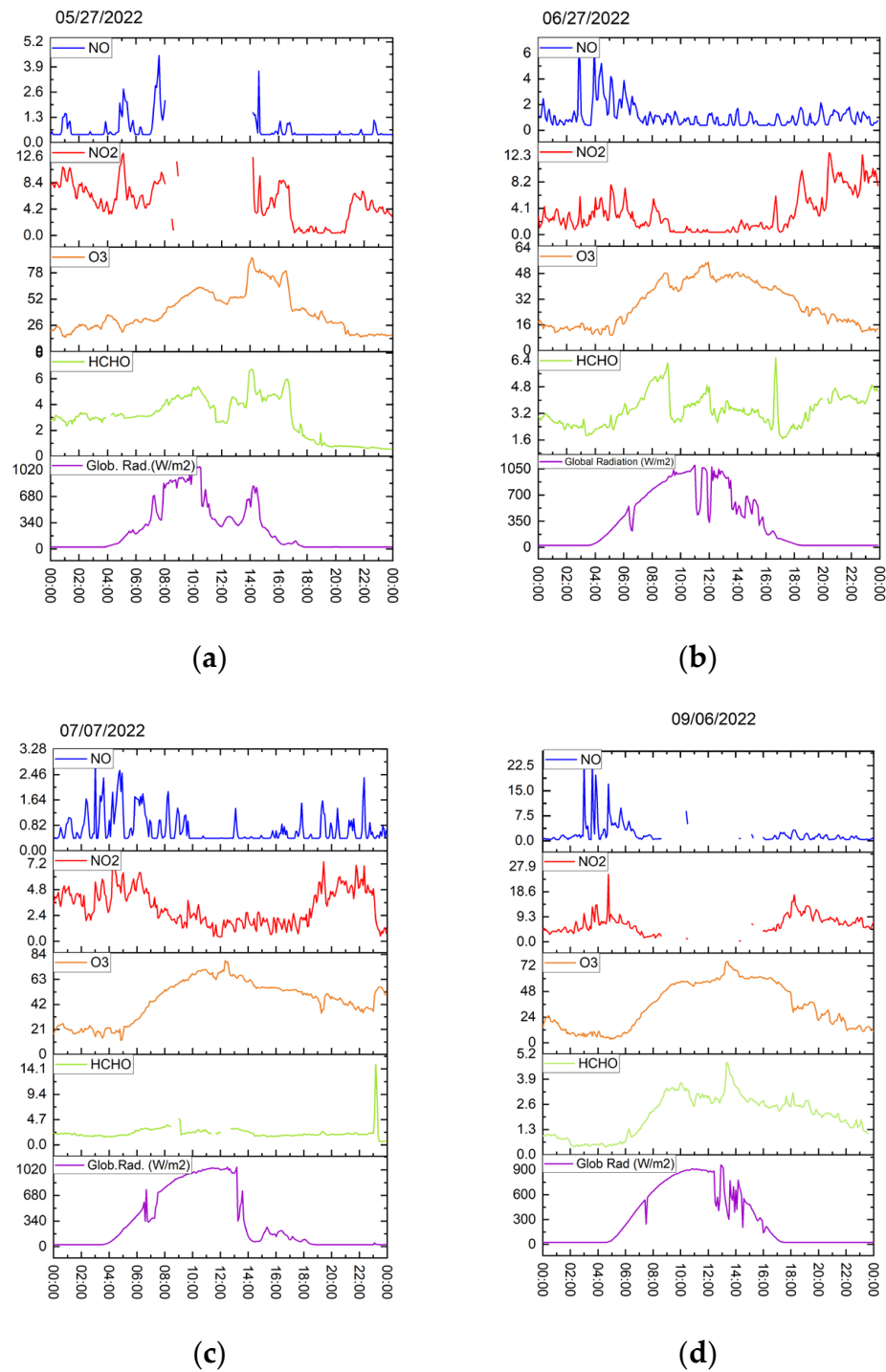


Figure 6. Cont.

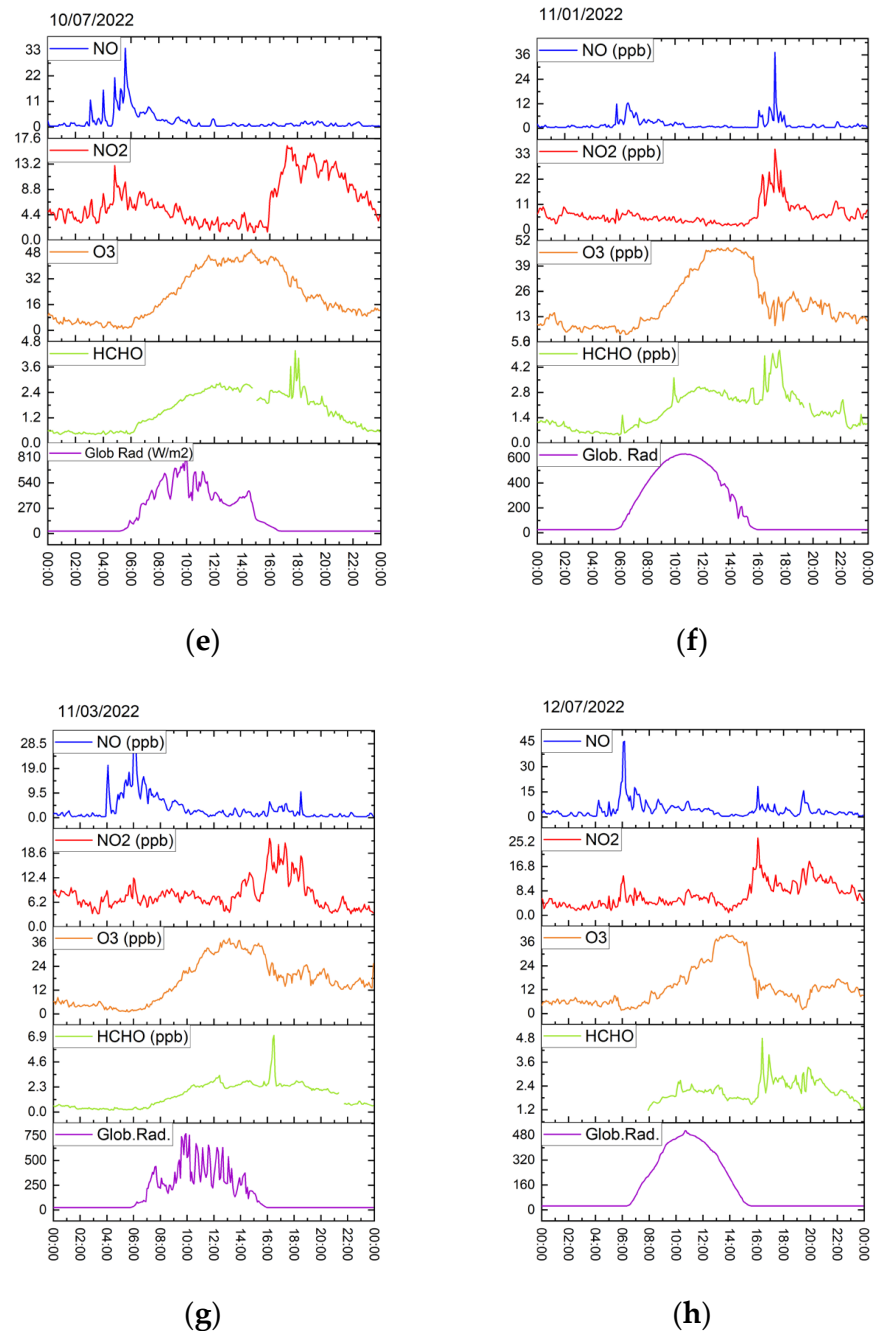
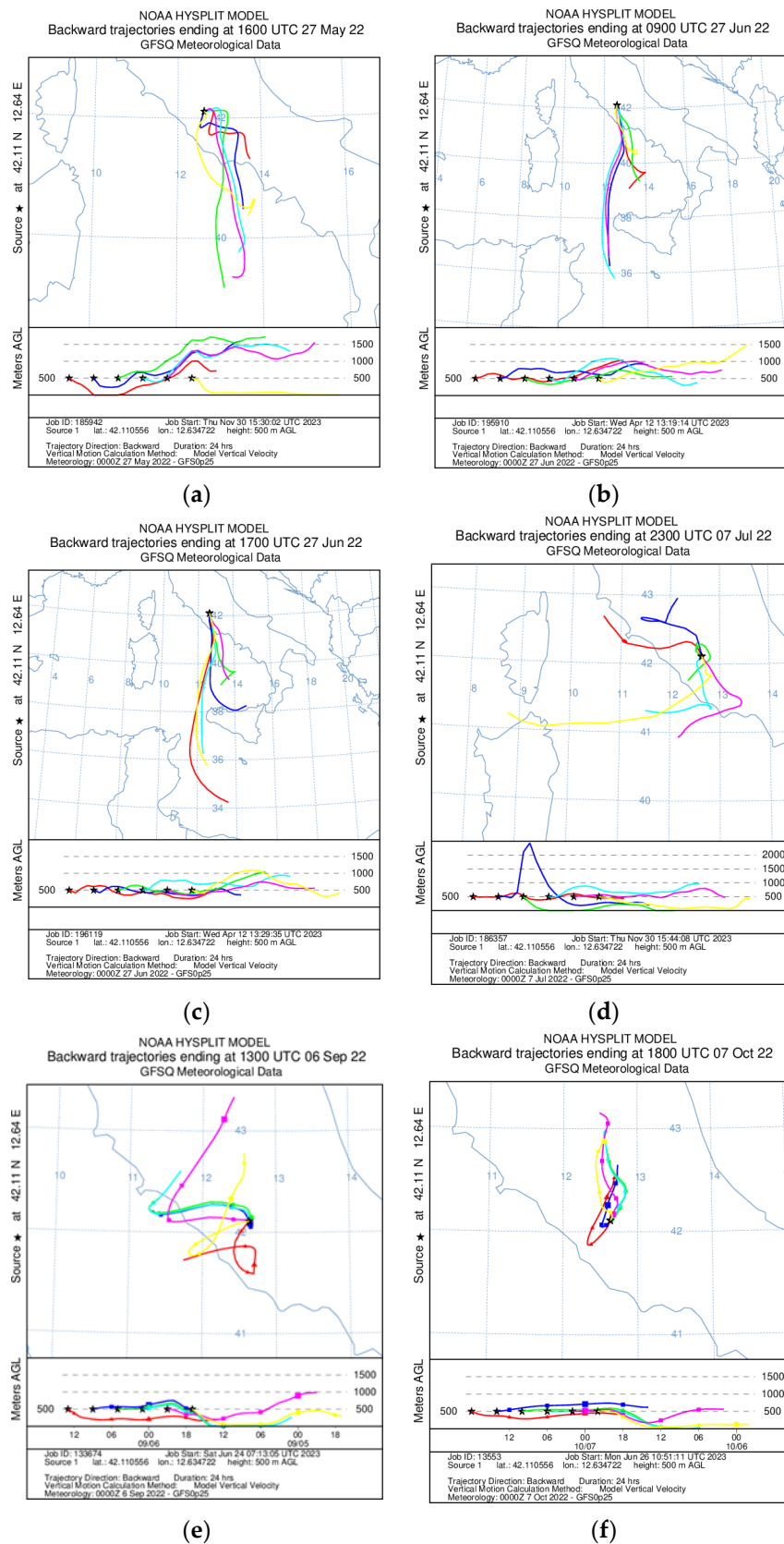


Figure 6. Pollutant trends (concentration in ppb averaged hourly) recorded on event days. The subfigures (a–h) refer to a different event day as reported above the plots. **Note:** Negative peaks of global radiation in summer mornings are due to a pole that casts its shadow daily.

On 3rd and 14th March, the HCHO peaks were recorded, respectively, at about 20.00 UTC time (7.2 ppb) and at 19.00 UTC (6.5 ppb), simultaneously to a NO₂ peak, local winds were coming from southeastern surrounding areas (see Figures S3g,h and S4h).

On 26th, 27th, and 28th May, the levels of HCHO increased. On average, during these three days, HCHO levels were higher (2.6 ppb) than the monthly average (1.4 ppb). The first events happened on 26th at 20.41 when 6.12 ppb of HCHO was measured, and on 27th May at 16.30, both the peaks overlapped to O₃ and also to NO₂ and NO peaks (see Figure 6a). The peak at 16.30 UTC time occurred just before a massive rain event in conditions of scarce solar radiation. The transport from southwestern nearby areas can be hypothesized on the basis of Figure 6a, and Figures S3j and S4j for both the events, on

a local scale, due to the weakness of the winds recorded (respectively of 0.78 m/s and 1.2 m/s). The other events recorded on 27th and 28th May were likely much more caused by the photochemical production effect and will be discussed later.



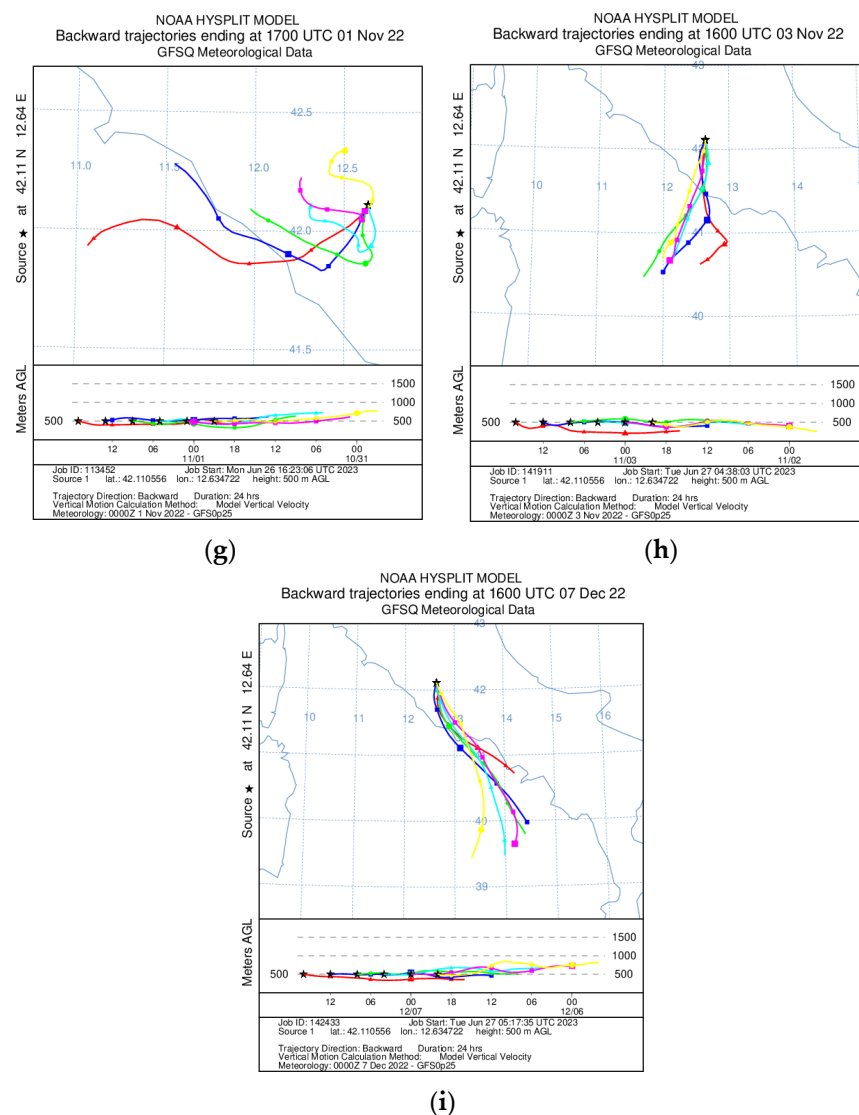


Figure 7. The 24 h backward trajectories relevant to the events. The subfigures (a–i) refer to the specific event, reported above the figure (the starting time of the 24 h backward trajectory corresponds to the occurrence hour of the event).

In summer, on 3rd August evening at 19.24, a peak of 5.8 ppb was observed along with a NO_2 peak. From the analysis of the polar plot in Figure S3t and S4t, it is apparent that the source, likely of primary nature, was in adjacent areas south of the monitoring site. In autumn, a few events were recorded during the late afternoon and evening, around 17.00 UTC time, on 7th October, 1st November, 3rd November, and 7th December. In all the cases, the sources were located south with respect to the measurement site (see Figures S3v–y and S4v–y). The provenance of the air masses, as evident from the backward trajectories in Figure 7f–i, was in almost all these autumn events from the south (varying from southeast to southwest). The peaks were always accompanied by NO_2 peaks, and on 1st November, also by NO peak (Figure 6f). The bivariate polar plots show that the winds during the events were weak (average wind speed and maxima ranging from 0.71 to 0.85 m/s and from 2.49 to 2.78 m/s) and coming from the south; stronger winds were recorded on 3rd November (average wind speed of 1.16 m/s and maximum 4.8 m/s). The event of 1st November, when All Saints Day is celebrated, differs from the others since NO peak was recorded as well. In this case, it is possible that fresh new emissions were released during the late afternoon also in relation to the celebration, whereas during the other events, the peaks were likely due to photochemically processed local air masses.

By considering the late summer and autumn data, it appears that the HCHO follows the trend of solar radiation as well as ozone, but due to solar radiation weakening over the whole period since the 1st November event, a bimodal distribution with a more evident late-afternoon peak was observed (Figure 6f).

The transport from the Rome metropolitan area can be hypothesized for three events that happened in summer on 27th June when at 16.41, an HCHO 6.6 ppb peak coincident with a peak of NO₂, suggesting a common source, was observed (see Figure 6b). Unfortunately, wind data are not available for the afternoon of 27th after 14.30 to better characterize the source location, but taking into account the backward trajectories reported in Figure 7b,c, the airmasses during 27th June were passing in Rome outskirts in the morning and at the eastern edge, in close proximity to the city, during the afternoon; therefore, the site was downwind of the city outskirts.

On 4th of July, two peaks were recorded at 11.30 (6.8 ppb), attributable to photochemical formation as discussed later, and at 19.35 (7.0 ppb). As can be observed in Figures S3q and S5b, the bivariate polar plots of HCHO and NO vs. the winds, recorded during the 4th of July, show that an increased concentration of both pollutants was likely associated with the transport from the southwest, from the roman urban area. During the 4th of July, a wildfire occurred on the northwestern edge of the city of Rome. This event was likely detectable by HCHO and NO levels.

In September, a single event was recorded on Tuesday the 6th when the HCHO concentration value reached 4.8 ppb at 13.30 UTC time; unfortunately, NO₂ and NO data during that period are not available. In any case, the event was likely due to transported air masses coming from southwestern areas with respect to the measurement site, as shown by the bivariate polar plot (in Figures S3u and S4u), where it is evident that the higher concentrations were associated with southwesterly winds.

The transport from Rome during the summer was due to the presence of sea breezes, which, entering inland, gradually decreased in strength [45,46] but could still be effective in transporting the urban plume downwind in the northeastern rural areas.

A photochemical pathway leading to increasing concentrations and peak events began on the last days of May, but can be clearly recognized in June and July.

On the 27th May, the evolution of the formaldehyde concentration profile in Figure 6a followed the trend of UV radiation, hence was likely due to photochemical processes, and the concentrations steadily grew from 8.30 to 10.30 UTC time. The first peak event (6.6 ppb) occurred at about 14.00, following the trend of global radiation and ozone trends, while mild breeze winds (3.9 m/s) were coming from the southwest (see Figure S3j). A gradual increase was also observed on 28th May when a 4.5 ppb peak was observed at 10.36 UTC time.

During the summer period, several HCHO peaks occurred in the month of June on days 3rd, 15th, 27th, and 28th. The peaks were in the range 5.9–7.1 ppb, the hour of appearance varied, on 3rd the maximum, occurred at 10.51 on 15th of June at 12.06 in both the cases, the trend agreed quite well with the O₃ one and with the global radiation, suggesting a photochemical production of both the pollutants.

The last days of June were, as already mentioned in Section 3.1, the hottest of the summer of 2022, and temperatures of 41.2 °C and 40.8 °C were recorded, respectively, on 27th and 28th of June. On 27th June, two HCHO peaks were observed, one in the morning at 9.06 and one in the afternoon at 16.41 (see Figure 6b). The former was likely due to photochemical formation, whereas the latter, as previously reported, was due to transport.

An increase during the morning was also observed on 28th of June, with a peak of 7.1 ppb recorded at 7.51. The following HCHO data between 9.26 and 15.26, unfortunately, are lost, and a more comprehensive discussion of the trends of the day is impossible. As reported by de Blas [20], the emissions of BVOCs are much more dependent on temperature than on radiation, so the last days of June were probably affected by two contemporary sources, one related to the biogenic hydrocarbons increased emissions and the other one to local, or in some cases, transported anthropogenic emissions.

In the month of July, HCHO maxima were found, particularly during the first week, on 4th, 5th, and 7th July. On 4th and 5th of July, both at about 11.30, two peaks were recorded, 6.8 ppb and 9.57 ppb, respectively, the latter followed by an almost equivalent 8.45 ppb peak at 12.00. In this case, the peaks are coincident with the maximum global radiation; therefore, they can be attributed to a photochemical mechanism of formation.

Other peaks observed were possibly caused by the occurrence of precipitations and stormy events. On 9th of June, a rain event happened at 8.50, and the presence of moisture likely increased HCHO concentration levels since this species is quite soluble in water and, therefore, can be released by the action of moisture on the sampling lines, producing an artifact peak. On the night of 7th July at 23.00 (UTC time), a sudden sharp peak of HCHO (15.0 ppb) was accompanied by a broader peak of O₃ reaching 54.8 ppb. During that night, a thunderstorm happened exactly around 23.00. Very strong north/northeasterly winds (see Figure S3s) were recorded at the site (wind speed maximum 16.1 m/s, average 10.7 m/s over the period 23.00–23.40), and lightning was reported over the area. Precipitations were abundant, and 16.2 mm of rain fell in about half an hour (from 23.10 to 23.45); consequently, the RH value increased rapidly from 62% to 98%. The cause of the two HCHO peaks differs since the 9th June one was likely an artifact, and it lasted only a few minutes, whereas the 7th July one lasted about 15–20 min during the stormy conditions described. Since there was a sudden change in wind direction, shifting suddenly from south to north, and speed within the peak event period, it can be concluded that the combination of the heavy rain and, on the whole, other meteorological parameters was responsible for the peak observed.

Regarding the effect of moisture in relation to heavy precipitations, apart from the two cited episodes, it was not really a concern during sampling over the whole year. This is also confirmed by the low correlation between rain and HCHO concentration (Pearson's *r* varying between -0.07 and 0 in the different seasons).

Nevertheless, in the literature, the issue of rainfall and HCHO atmospheric scavenging was discussed by Largiuni [25], and details of sampling artifacts due to inlet design were reported by Wert et al., 2002 [54]. In particular, the former underlines the discrepancy between HCHO atmospheric concentrations calculated on the basis of gas–liquid equilibria and actual values measured, concluding that wet deposition largely depends on the amount of precipitation in a given period of time and also on other factors.

On the other hand, the accidental ingestion of liquid water by inlets may cause measurement errors. Wert et al. report on the comparison of different inlet layouts used during aircraft campaigns. Furthermore, it should be considered that the meteorological conditions encountered during aircraft sampling are more extreme than the ones normally present on the ground.

On the basis of the analysis performed, it is evident that the occurrence of peak events was observed mainly during winter and summer, whereas in spring and autumn, very low and low values of HCHO concentration were measured, respectively. In spring, the effect of photochemical processes, though the global radiation increased starting from April (see Table 1), became more evident on the last days of May and July. During the month of April, the temperature kept showing low values (minimum 2.4 °C), particularly during the first hours of the morning. At the same time, the development of photochemical processes of the formation of certain species, such as O₃ and HCHO, was initiated, but the HCHO concentration level did not show appreciable peak events. Opposite to what happened during July, reported earlier in this section, due to the dependence on the temperature of hydrocarbon emissions by biogenic sources, the evolution of photochemical production at the Liberti site was partially inhibited during the first two spring months.

3.3. Formaldehyde to Nitrogen Dioxide Ratio as Photochemical Indicator (PI)

The use of photochemical indicators (PI) has been proposed in several studies and widely employed to associate the ratios of different secondary products with the O₃/NO_x/VOC budget. Various approaches were attempted, as reported by Liu [55], the ratios of VOC/NO_x, H₂O₂/HNO₃, HCHO/NO₂ or HCHO/NO_y, or also O₃/NO_y, O₃/HNO₃ have been used

to assess the dependence of O₃ formation either by NO_x or VOC pollutants. The main drawback of such indices is that the threshold values given by models will differ depending on the environmental conditions. Therefore, there is no standard value for these thresholds, and their applicability in certain cases can be restricted only to specific O₃ concentration ranges.

Despite these limits and uncertainties, the ratio of HCHO to NO₂ was calculated over the dataset to assess the feasibility of getting some information on the regime governing O₃ formation at the site under study.

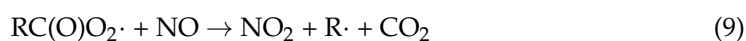
As is well known, the formation of O₃ in clean air is in a stable state [55,56]:



The presence of VOC species of anthropogenic or natural origin changes this stable state through a series of reactions:



In the case of aldehydes:



Other important reactions are:



Termination reactions can be:



There are two concurrent mechanisms through which the buildup of ozone concentration can occur: the production of oxygen radicals by NO₂ with solar radiation (reaction 1) and the conversion of NO to NO₂ by VOCs through the HO₂· and RO₂·, which convert NO to NO₂, inhibiting the titration of NO by O₃, leading to a further increase in O₃. When the VOC/NO_x ratio is low, the termination reaction is the production of nitric acid (HNO₃), the

concentration of $\text{OH}\cdot$, and, as a consequence, the oxidation of NO decreases. Hence, the formation of NO_2 in this regime is due to the NO oxidation by peroxy radicals produced by VOC precursors. Therefore, an increase in VOCs will correspond to an increment of O_3 (VOC-limited chemistry). If the VOC/NO_x ratio is high, reaction (13) is the termination and the lack of NO to be oxidized by peroxy radicals, which brings about the accumulation of ozone. Thus, the concentration of nitrogen oxides determines the levels of ozone under this regime (NO_x -limited chemistry).

By calculating the ratio HCHO/NO_2 on the available data on a seasonal basis, the relative box plot graphs are reported in Figure 8. It was found that the mean value was close to 1 in spring and summer, whereas it was 0.38 and 0.25, respectively, during winter and autumn.

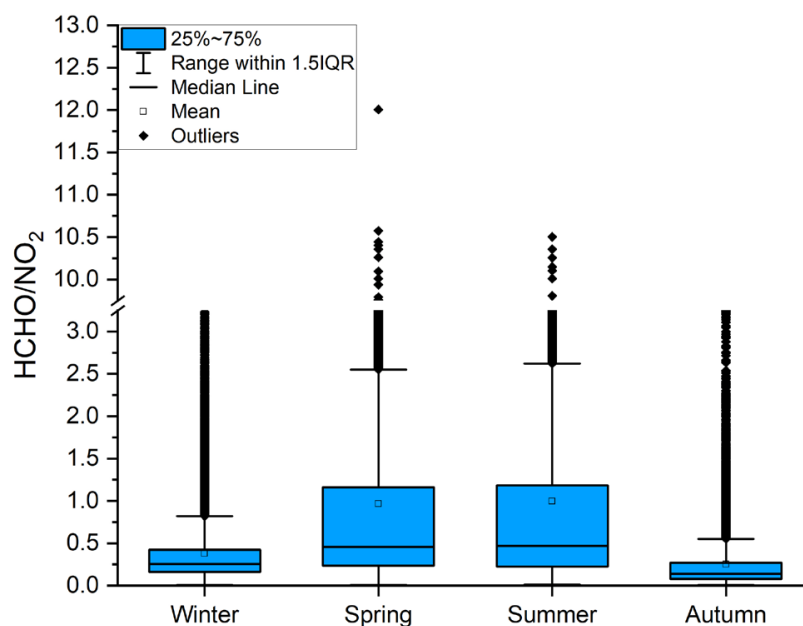


Figure 8. Box plot graphs of seasonal distribution of HCHO/NO_2 ratios.

The data are also represented graphically in Figure 9 for the different seasons examined on an hourly basis. It is possible to observe that the seasonal daily cycles of the ratio showed higher values in spring and summer at noon, when ratios ranging from 2.5 to 2.7 were calculated, whereas in autumn and winter, they ranged from 0.5 to 0.6. As expected, the summer months of June and July (see Figure S6) showed the highest values at 12.00 UTC, corresponding to 14.00 local time, when the emission of biogenic VOCs was likely more intense.

As reported by Liu [55] and references therein, the transition between VOC-limited and NO_x -limited regimes usually occurs in summer when the ratio is equal to 1. However, the same authors also report on the variability of the thresholds, discriminating different regimes affecting ozone formation, of some of the photochemical indicators such as HCHO/NO_2 ratio, as well as other concerns raised by Li et al. [57] about the effect of HCHO primary emissions on this ratio and its susceptibility to meteorological parameters.

As already mentioned, the exact threshold values at which different regimes rule O_3 formation depend on many concurrent factors; therefore, it is not possible to indicate the dominant regime according to the HCHO/NO_2 ratio at different times/hours, but it seems reasonable to conclude that during summer central hours of the day, the formation of ozone at the rural station was NO_x -limited (higher value of the ratio indicate a limitation due to NO_x).

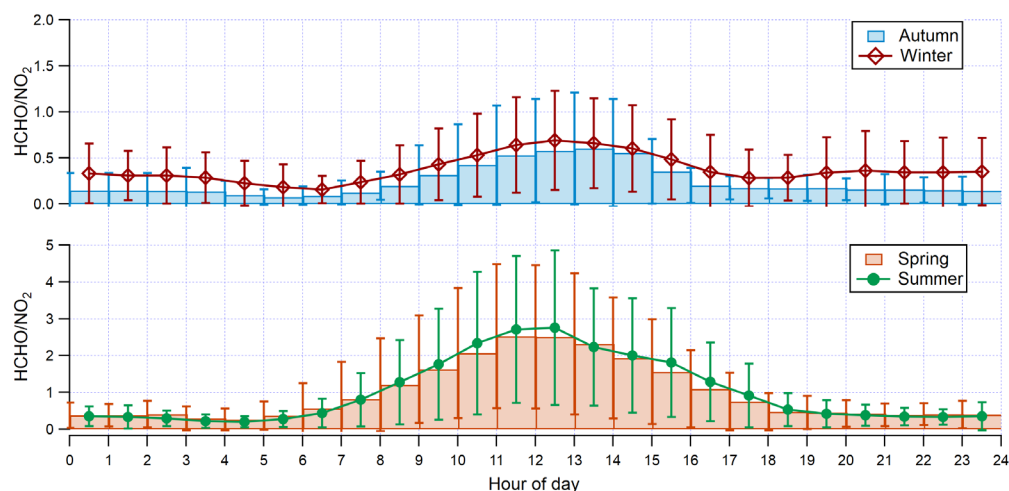


Figure 9. Trends of HCHO/NO₂ ratios hourly averages over the different seasons of the period investigated.

4. Conclusions

The availability of real-time data for HCHO has allowed an extended evaluation compared to former data [32,47,48] collected at the same site. The comprehensive monitoring, which included meteorological parameters and other pollutant concentration data, merged with information on backward trajectories of air masses, has provided a quite complex picture of the occurrence and the mechanisms of formation of HCHO, including peak events. The data collected suggest a predominance of primary sources impact in the winter–early spring months (until April) and autumn, whereas a secondary origin was predominant in the rest of the period investigated. Occasional episodes, such as wildfires and certain meteorological events, in particular a thunderstorm, had an impact on HCHO concentrations. The site examined was sometimes impacted by the nearby urban anthropic pressure of Rome (about 30 km southeast of the station), but in many cases, particularly during the summer months, the influence of the natural background surrounding the site was evident. The emission of biogenic VOCs by the vegetation was studied over the years [58], but due to the changed meteorological conditions, which cause longer hot and dry periods and more extreme events, the overall characteristics of the site have changed, as well as in other rural areas.

The regime dominating ozone formation at the site was also investigated through the calculation of the HCHO/NO₂ ratio. The values found in June and July during the central hours of the day point to a NO_x-dominated regime since, during these periods, increased concentrations of biogenic VOCs can normally be found at rural sites, being likely the predominant hydrocarbons. Generally speaking, accounting for the vegetation contribution to the formation of air pollution, especially for photochemically produced species, such as HCHO and O₃, is of increasing importance, and modeling can be a viable tool [59].

A future study concerning the biogenic VOCs load at the site is foreseen, as well as the extension to other carbonyls, with the view of obtaining a more complete investigation and providing a more precise description of the local sources.

The possibility of considering these findings and other future data available at the Liberti Observatory, along with satellite-retrieved data, is envisaged for the future. The integration of ground-based and satellite (TROPOMI sensor) data, indeed, would be meaningful if the dataset comprises several seasonal periods. Nevertheless, it should be mentioned that in the literature, different authors highlight several issues concerning the calculation of this ratio using satellite data.

Supplementary Materials: The following supporting information can be downloaded at: <https://www.mdpi.com/article/10.3390/atmos14121833/s1>, Figure S1: Wind roses of the period investigated plotted on a monthly basis; Figure S2: Diurnal variations of the pollutants measured

monthly: above HCHO vs. O₃, below NO₂ vs. NO; Figure S3: Bivariate polar plots of the days with HCHO peak occurrence vs. wind data (on left axis windspeed in m/s); Figure S4: NO₂ Bivariate polar plots of the days with HCHO peak occurrence (on left axis windspeed in m/s); Figure S5: NO bivariate polar plots of some of the days with HCHO peak occurrence (on left axis windspeed in m/s); Figure S6: Trends of HCHO/NO₂ ratios hourly averages over the different months of the period investigated.

Author Contributions: Conceptualization, data curation, writing—original draft preparation F.V.; data curation, writing—review and editing, C.B.; conceptualization, writing—review and editing, A.I. (Antonietta Ianniello); validation, software, G.E. and M.M.; data curation, methodology, writing—review and editing, A.I. (Andrea Imperiali). All authors have read and agreed to the published version of the manuscript.

Funding: This research received no external funding.

Data Availability Statement: The data presented in this study are available on request from the corresponding author. The data are not publicly available due to the fact that an accessible repository was not yet created.

Acknowledgments: The authors thank Marco Giusto for his support in meteorological data treatment.

Conflicts of Interest: The authors declare no conflict of interest.

References

1. Seinfeld, J.H.; Pandis, S.N. *Atmospheric Chemistry and Physics: From Air Pollution to Climate Change*, 3rd ed.; John Wiley & Sons: Hoboken, NJ, USA, 2016; ISBN 9781118947401.
2. International Agency for Research on Cancer (IARC). *IARC Monographs on the Evaluation of Carcinogenic Risks to Humans: Formaldehyde, 2-Butoxyethanol and 1-Tert-Butoxypropan-2-ol. Volume 88*; International Agency for Research on Cancer: Lyon, France, 2006.
3. Commission Regulation (EU) 2015/491 of 23 March 2015 Amending Regulation (EU) No 605/2014 Amending, for the Purposes of Introducing Hazard and Precautionary Statements in the Croatian Language and Its Adaptation to Technical and Scientific Progress, Regulation (EC) No 1272/2008 of the European Parliament and of the Council on Classification, Labelling and Packaging of Substances and Mixtures. Available online: <https://eur-lex.europa.eu/legal-content/EN/TXT/PDF/?uri=CELEX:32015R0491&from=PL> (accessed on 6 December 2023).
4. Protano, C.; Buomprisco, G.; Cammalleri, V.; Pocino, R.N.; Marotta, D.; Simonazzi, S.; Cardoni, F.; Petyx, M.; Iavicoli, S.; Vitali, M. The Carcinogenic Effects of Formaldehyde Occupational Exposure: A Systematic Review. *Cancers* **2022**, *14*, 165. [[CrossRef](#)] [[PubMed](#)]
5. Available online: <https://www.epa.gov/sites/default/files/2016-09/documents/formaldehyde.pdf> (accessed on 6 December 2023).
6. Birmili, W.; Daniels, A.; Bethke, R.; Schechner, N.; Brasse, G.; Conrad, A.; Kolossa-Gehring, M.; Debiak, M.; Hurraß, J.; Uhde, E.; et al. Formaldehyde, aliphatic aldehydes (C₂–C₁₁), furfural, and benzaldehyde in the residential indoor air of children and adolescents during the German Environmental Survey 2014–2017. *Indoor Air* **2022**, *32*, e12927. [[CrossRef](#)] [[PubMed](#)]
7. Trocquet, C.; Lara-Ibeas, I.; Schulz, A.; Bernhardt, P.; Cormerais, B.; Englaro, S.; Le Calvé, S. Continuous aldehydes monitoring in primary schools in France: Evaluation of emission sources and ventilation practices over 5 weeks. *Atmos. Pollut. Res.* **2021**, *12*, 340–351. [[CrossRef](#)]
8. Bhardwaj, N.; Kelsch, A.; Eatough, D.J.; Thalman, R.; Daher, N.; Kelly, K.; Jaramillo, I.C.; Hansen, J.C. Sources of Formaldehyde in Bountiful, Utah. *Atmosphere* **2021**, *12*, 375. [[CrossRef](#)]
9. Dienhart, D.; Crowley, J.N.; Bourtsoukidis, E.; Edtbauer, A.; Eger, P.G.; Harder, H.; Hottmann, B.; Martinez, M.; Parchatka, U.; Paris, J.D.; et al. Measurement report: Observation-based formaldehyde production rates and their relation to OH reactivity around the Arabian Peninsula. *Atmos. Chem. Phys.* **2021**, *21*, 17373–17388. [[CrossRef](#)]
10. Liu, Q.; Gao, Y.; Huang, W.; Ling, Z.; Wang, Z.; Wang, X. Carbonyl compounds in the atmosphere: A review of abundance, source and their contributions to O₃ and SOA formation. *Atmos. Res.* **2022**, *274*, 106184. [[CrossRef](#)]
11. Marcon, A.; Panunzi, S.; Stafoggia, M.; Badaloni, C.; de Hoogh, K.; Guarda, L.; Locatelli, F.; Silocchi, C.; Ricci, P.; Marchetti, P. Spatial variability of nitrogen dioxide and formaldehyde and residential exposure of children in the industrial area of Viadana, Northern Italy. *Environ. Sci. Pollut. Res.* **2021**, *28*, 28096–28106. [[CrossRef](#)]
12. Zhang, H.; Zheng, Z.; Yu, T.; Liu, C.; Qian, H.; Li, J. Seasonal and diurnal patterns of outdoor formaldehyde and impacts on indoor environments and health. *Environ. Res.* **2022**, *205*, 112550. [[CrossRef](#)]
13. Parrish, D.D.; Ryerson, T.B.; Mellqvist, J.; Johansson, J.; Fried, A.; Richter, D.; Walega, J.G.; Washenfelder, R.A.; de Gouw, J.A.; Peischl, J.; et al. Primary and secondary sources of formaldehyde in urban atmospheres: Houston Texas region. *Atmos. Chem. Phys.* **2012**, *12*, 3273–3288. Available online: <https://www.atmos-chem-phys.net/12/3273/2012> (accessed on 6 December 2023). [[CrossRef](#)]

14. Qian, X.; Shen, H.; Chen, Z. Characterizing summer and winter carbonyl compounds in Beijing atmosphere. *Atmos. Environ.* **2019**, *214*, 116845. [CrossRef]
15. Green, J.R.; Fiddler, M.N.; Fibiger, D.L.; Erin, E.; McDuffie, E.E.; Aquino, J.; Campos, T.; Shah, V.; Jaeglé, L.; Thornton, J.A.; et al. Wintertime Formaldehyde: Airborne Observations and Source Apportionment Over the Eastern United States. *J. Geophys. Res. Atmos.* **2021**, *126*, e2020JD033518. [CrossRef]
16. Preunkert, S.; Legrand, M.; Frey, M.M.; Kukui, A.; Savarino, J.; Gallée, H.; King, M.; Jourdain, B.; Vicars, W.; Helmig, D. Formaldehyde (HCHO) in air, snow, and interstitial air at Concordia (East Antarctic Plateau) in summer. *Atmos. Chem. Phys.* **2015**, *15*, 6689–6705. [CrossRef]
17. Leuchner, M.; Ghasemifard, H.; Lüpke, M.; Ries, L.; Schunk, C.; Menzel, A. Seasonal and Diurnal Variation of Formaldehyde and its Meteorological Drivers at the GAW Site Zugspitze. *Aerosol Air Qual. Res.* **2016**, *16*, 801–815. [CrossRef]
18. Rocco, M.; Colomb, A.; Baray, J.-L.; Amelynck, C.; Verreyken, B.; Borbon, A.; Pichon, J.-M.; Bouvier, L.; Schoon, N.; Gros, V.; et al. Analysis of Volatile Organic Compounds during the OCTAVE Campaign: Sources and Distributions of Formaldehyde on Reunion Island. *Atmosphere* **2020**, *11*, 140. [CrossRef]
19. Aakko-Saksa, P.; Koponen, P.; Roslund, P.; Laurikko, J.; Nylund, N.-O.; Karjalainen, P.; Rönkkö, T.; Timonen, H. Comprehensive emission characterisation of exhaust from alternative fuelled cars. *Atmos. Environ.* **2020**, *236*, 117643. [CrossRef]
20. de Blas, M.; Ibáñez, P.; García, J.A.; Gómez, M.C.; Navazo, M.; Alonso, L.; Durana, N.; Iza, J.; Gangoiti, G.; Sáez de Cámara, E. Summertime high resolution variability of atmospheric formaldehyde and non-methane volatile organic compounds in a rural background area. *Sci. Total Environ.* **2019**, *647*, 862–877. [CrossRef] [PubMed]
21. Luecken, D.J.; Hutzell, W.T.; Strum, M.L.; Pouliot, G.A. Regional Sources of Atmospheric Formaldehyde and Acetaldehyde, and Implications for Atmospheric Modeling. *Atmos. Environ.* **2012**, *47*, 477–490. [CrossRef]
22. Salthammer, T. Formaldehyde in the ambient atmosphere: From an indoor pollutant to an outdoor pollutant? *Angew. Chem. Int. Ed.* **2013**, *52*, 3320–3327. [CrossRef]
23. Cheng, P.; Liu, Z.; Feng, Y.; Han, Y.; Peng, Y.; Cai, J.; Chen, Y. Emission characteristics and formation pathways of carbonyl compounds from the combustion of biomass and their cellulose, hemicellulose, and lignin at different temperatures and oxygen concentrations. *Atmos. Environ.* **2022**, *291*, 119387. [CrossRef]
24. Solberg, S.; Dye, C.; Walker, S.-E.; Simpson, D. Long-term measurements and model calculations of formaldehyde at rural European monitoring sites. *Atmos. Environ.* **2001**, *35*, 195–207. [CrossRef]
25. Largiuni, O.; Giacomelli, M.C.; Piccardi, G. Concentration of Peroxides and Formaldehyde in Air and Rain and Gas-Rain Partitioning. *J. Atmos. Chem.* **2002**, *41*, 1–20. [CrossRef]
26. Balzani Lööf, J.M.; Henne, S.; Legreid, G.; Staehelin, J.; Reimann, S.; Prévôt, A.S.H.; Steinbacher, M.; Vollmer, M.K. Estimation of background concentrations of trace gases at the Swiss Alpine site Jungfraujoch (3580 m asl). *J. Geophys. Res. Atmos.* **2008**, *113*, D22. [CrossRef]
27. Wang, X.; Wang, H.; Wang, S. Ambient formaldehyde and its contributing factor to ozone and OH radical in a rural area. *Atmos. Environ.* **2010**, *44*, 2074–2078. [CrossRef]
28. Available online: <https://eur-lex.europa.eu/legal-content/EN/TXT/DOC/?uri=CELEX:52022PC0542> (accessed on 6 December 2023).
29. Available online: <https://demo.istat.it/app/?a=2022&i=D7B> (accessed on 6 December 2023).
30. Ciccioli, P.; Brancaleoni, E.; Frattoni, M. Chapter 5—Reactive Hydrocarbons in the Atmosphere at Urban and Regional Scales. In *Reactive Hydrocarbons in the Atmosphere*; Hewitt, C.N., Ed.; Academic Press: Cambridge, MA, USA, 1999; pp. 159–207. [CrossRef]
31. Brines, M.; Dall’Osto, M.; Beddows, D.C.S.; Harrison, R.M.; Gómez-Moreno, F.; Núñez, L.; Artíñano, B.; Costabile, F.; Gobbi, G.P.; Salimi, F.; et al. Traffic and nucleation events as main sources of ultrafine particles in high-insolation developed world cities. *Atmos. Chem. Phys.* **2015**, *15*, 5929–5945. [CrossRef]
32. Possanzini, M.; Tagliacozzo, G.; Cecinato, A. Ambient Levels and Sources of Lower Carbonyls at Montelibretti, Rome (Italy). *Water Air Soil Pollut.* **2007**, *183*, 447–454. [CrossRef]
33. Carbone, C.; Decesari, S.; Mircea, M.; Giulianelli, L.; Finessi, E.; Rinaldi, M.; Fuzzi, S.; Marinoni, A.; Duchi, R.; Perrino, C.; et al. Size-resolved aerosol chemical composition over the Italian Peninsula during typical summer and winter conditions. *Atmos. Environ.* **2010**, *44*, 5269–5278. [CrossRef]
34. Yttri, K.E.; Simpson, D.; Bergström, R.; Kiss, G.; Szidat, S.; Ceburnis, D.; Eckhardt, S.; Hueglin, C.; Nøjgaard, J.K.; Perrino, C.; et al. The EMEP Intensive Measurement Period campaign, 2008–2009: Characterizing carbonaceous aerosol at nine rural sites in Europe. *Atmos. Chem. Phys.* **2019**, *19*, 4211–4233. [CrossRef]
35. Nash, T. The colorimetric estimation of formaldehyde by means of the Hantzsch reaction. *Biochem. J.* **1953**, *55*, 416–421. [CrossRef]
36. Kelly, T.J.; Fortune, C.R. Continuous monitoring of gaseous formaldehyde using an improved fluorescence approach. *Int. J. Environ. Anal. Chem.* **1994**, *54*, 249–263. [CrossRef]
37. Available online: <https://www.aero-laser.de/fileadmin/downloads/AL4021-manual-Rev.2.2.pdf> (accessed on 6 December 2023).
38. Hak, C.; Pundt, I.; Trick, S.; Kern, C.; Platt, U.; Dommen, J.; Ordóñez, C.; Prévôt, A.S.H.; Junkermann, W.; Astorga-Lloréns, C.; et al. Intercomparison of four different in-situ techniques for ambient formaldehyde measurements in urban air. *Atmos. Chem. Phys.* **2005**, *5*, 2881–2900. [CrossRef]
39. Hladová, M.; Martinka, J.; Rantuch, P.; Necas, A. Review of spectrophotometric methods for determination of formaldehyde. *J. Slovak Univ. Technol.* **2019**, *27*, 105–120. [CrossRef]

40. Junkermann, W.; Burger, J.M. A new portable Instrument for Continuous Measurement of Formaldehyde in Ambient Air. *J. Atmos. Ocean. Technol.* **2006**, *23*, 38–45. [CrossRef]
41. EN 14625:2012; Air, CEN Ambient. Standard Method for the Measurement of the Concentration of Ozone by Ultraviolet Photometry. European Committee for Standardization: Brussels, Belgium, 2012.
42. EN 14211:2012; Air, CEN Ambient. Ambient Air—Standard Method for the Measurement of the Concentration of Nitrogen Dioxide and Nitrogen Monoxide by Chemiluminescence. European Committee for Standardization: Brussels, Belgium, 2012.
43. Stein, A.F.; Draxler, R.R.; Rolph, G.D.; Stunder, B.J.B.; Cohen, M.D.; Ngan, F. NOAA’s HYSPLIT atmospheric transport and dispersion modeling system. *Bull. Amer. Meteor. Soc.* **2015**, *96*, 2059–2077. [CrossRef]
44. Di Bernardino, A.; Iannarelli, A.M.; Diémoz, H.; Casadio, S.; Cacciani, M.; Siani, A.M. Analysis of two-decade meteorological and air quality trends in Rome (Italy). *Theor. Appl. Climatol.* **2022**, *149*, 291–307. [CrossRef] [PubMed]
45. Di Bernardino, A.; Mazzarella, V.; Pecci, M.; Casasanta, G.; Cacciani, M.; Ferretti, R. Interaction of the Sea Breeze with the Urban Area of Rome: WRF Mesoscale and WRF Large-Eddy Simulations Compared to Ground-Based Observations. *Bound. Layer Meteorol.* **2022**, *185*, 333–363. [CrossRef]
46. Bassani, C.; Vichi, F.; Esposito, G.; Falasca, S.; Di Bernardino, A.; Battistelli, F.; Casadio, S.; Iannarelli, A.M.; Ianniello, A. Characterization of Nitrogen Dioxide Variability Using Ground-Based and Satellite Remote Sensing and In Situ Measurements in the Tiber Valley (Lazio, Italy). *Remote Sens.* **2023**, *15*, 3703. [CrossRef]
47. Possanzini, M.; Di Palo, V.; Brancaleoni, E.; Frattoni, M.; Ciccio, P. A train of carbon and DNPH-coated cartridges for the determination of carbonyls from C1 to C12 and emission samples. *Atmos. Environ.* **2000**, *34*, 5311–5318. [CrossRef]
48. Possanzini, M.; Di Palo, V.; Cecinato, A. Sources and photodecomposition of formaldehyde and acetaldehyde in Rome ambient air. *Atmos. Environ.* **2002**, *36*, 3195–3201. [CrossRef]
49. Zhang, K.; Batterman, S. Air pollution and health risks due to vehicle traffic. *Sci. Total Environ.* **2013**, *450–451*, 307–316. [CrossRef]
50. Blanchard, C.L.; Tanenbaum, S.J. Differences between Weekday and Weekend Air Pollutant Levels in Southern California. *J. Air Waste Manag.* **2003**, *53*, 816–828. [CrossRef]
51. Hassan, S.K.; El-Abssawy, A.A.; Khoder, M.I. Effect of Seasonal Variation on the Levels and Behaviours of Formaldehyde in the Atmosphere of a Suburban Area in Cairo, Egypt. *Asian J. Atmos. Environ. (AJAE)* **2018**, *12*, 356–368. [CrossRef]
52. Biswas, M.S.; Mahajan, A.S. Year-long Concurrent MAX-DOAS Observations of Nitrogen Dioxide and Formaldehyde at Pune: Understanding Diurnal and Seasonal Variation Drivers. *Aerosol Air Qual. Res.* **2021**, *21*, 200524. [CrossRef]
53. Carslaw, D.; Beevers, S. Characterising and understanding emission sources using bivariate polar plots and k-means clustering. *Environ. Model. Softw.* **2013**, *40*, 325–329. [CrossRef]
54. Wert, B.P.; Fried, A.; Henry, B.; Cartier, S. Evaluation of inlets used for the airborne measurement of formaldehyde. *J. Geophys. Res.* **2002**, *107*, ACH-3. [CrossRef]
55. Liu, C.; Shi, K. A review on methodology in O₃-NO_x-VOC sensitivity study. *Environ. Pollut.* **2021**, *291*, 118249. [CrossRef] [PubMed]
56. Jenkin, M.E.; Clemitshaw, K.C. Ozone and other secondary photochemical pollutants: Chemical processes governing their formation in the planetary boundary layer. *Atmos. Environ.* **2000**, *34*, 2499–2527. [CrossRef]
57. Li, X.; Qin, M.; Li, L.; Gong, K.; Shen, H.; Li, J.; Hu, J. Examining the implications of photochemical indicators for O₃-NO_x-VOC sensitivity and control strategies: A case study in the Yangtze River Delta (YRD), China. *Atmos. Chem. Phys.* **2022**, *22*, 14799–14811. [CrossRef]
58. Fares, S.; Mereu, S.; Scarascia Mugnozza, G.; Vitale, M.; Manes, F.; Frattoni, M.; Ciccio, P.; Gerosa, G.; Loreto, F. The ACCENT-VOCBAS field campaign on biosphere-atmosphere interactions in a Mediterranean ecosystem of Castelporziano (Rome): Site characteristics, climatic and meteorological conditions, and eco-physiology of vegetation. *Biogeosciences* **2009**, *6*, 1043–1058. Available online: <https://www.biogeosciences.net/6/1043/2009/> (accessed on 6 December 2023). [CrossRef]
59. Ciccio, P.; Silibello, C.; Finardi, S.; Pepe, N.; Ciccio, P.; Rapparini, F.; Neri, L.; Fares, S.; Brilli, F.; Mircea, M.; et al. The potential impact of biogenic volatile organic compounds (BVOCs) from terrestrial vegetation on a Mediterranean area using two different emission models. *Agric. For. Meteorol.* **2023**, *328*, 109255. [CrossRef]

Disclaimer/Publisher’s Note: The statements, opinions and data contained in all publications are solely those of the individual author(s) and contributor(s) and not of MDPI and/or the editor(s). MDPI and/or the editor(s) disclaim responsibility for any injury to people or property resulting from any ideas, methods, instructions or products referred to in the content.